Domain regime in two-dimensional disordered vortex matter

Mahesh Chandran,* R. T. Scalettar, and G. T. Zimányi
Department of Physics, University of California, Davis, California 95616, USA
(Received 28 July 2003; revised manuscript received 18 September 2003; published 30 January 2004)

A detailed numerical study of the real-space configuration of vortices in disordered superconductors using two-dimensional London-Langevin model is presented. The magnetic field B is varied between 0 and B_{c2} for various pinning strengths Δ. For weak pinning, an inhomogeneous disordered vortex matter is observed, in which the topologically ordered vortex lattice survives in large domains. The majority of the dislocations in this state are confined to the grain boundaries/domain walls. Such quasiordered configurations are observed in the intermediate fields, and we refer it as the domain regime (DR). The DR is distinct from the low-field and the high-fields amorphous regimes which are characterized by a homogeneous distribution of defects over the entire system. Analysis of the real-space configuration suggests domain-wall roughening as a possible mechanism for the crossover from the DR to the high-field amorphous regime. The DR also shows a sharp crossover to the high-temperature vortex liquid phase. The domain size distribution and the roughness exponent of the lattice in the DR are also calculated. The results are compared with some of the recent Bitter decoration experiments.

DOI: 10.1103/PhysRevB.69.024526 PACS number(s): 74.25.Qt, 74.25.Sv

I. INTRODUCTION

The vortex state in type-II superconductors is a paradigm for studying the effect of quenched disorder in condensed matter. Over the last decade, much of the effort has been made on characterizing the various phases of the vortex state as a function of the magnetic field B and the temperature T. For three-dimensional (3D) vortex system,[1] three phases have been identified unambiguously:[2–4] the Bragg glass (BG) with quasi-long-range order, the amorphous vortex glass (VG), and the vortex liquid (VL). The VG and the VL are distinguished by their superconducting and ohmic responses, respectively. Experiments in high-T_c superconductors suggest that the BG phase appears in the low-B and low-T region, whereas the VG phase occupies the high-B and low-T region of the B-T phase diagram. The VL phase appears close to the upper critical field $B_{c2}(T)$.

The first detailed calculation of the real-space structure of the vortex lattice in the presence of quenched impurities[5] was carried out by Larkin and Ovchinnikov[6] (LO). The LO theory assumes that for the weak pinning, the vortex lattice is coherently pinned within a volume V_c. Beyond V_c, the effect of impurities dominates and the long-range positional order is lost. It was further proposed that when the vortex displacement becomes of the order of lattice constant, topological defects (dislocations in $D=2$ and dislocation loops in $D=3$) are generated.[7] Later calculations by Giamarchi and Le Doussal[3,8] (GLD) showed that the LO calculation overestimates the effect of impurities at large distances and the vortex displacement grows only logarithmically (for 3D vortex system). The positional correlation decays as $C(r) \sim 1/r^{\eta}$, where η is a nonuniversal exponent.[9] The quasi-long-range $C(r)$ leads to a topologically ordered phase (the Bragg glass), which is stable with respect to the formation of defects.[10] On increasing B (or the pinning strength), the LO and GLD theories predict proliferation of topological defects, thus forming the VG at high fields.[11] The transition between the BG and the high-field VG is predicted to be of first order.[12–15] The BG also undergoes a melting transition to VL on increasing T.

In $D=2$, the BG phase is unstable to the formation of dislocations and the positional quasi-long-range order is destroyed.[16,17] However, for weak pinning and at low temperatures, the unbound dislocations appear only at large length scale $\xi_D \gg R_a$, where R_a is the ''random manifold'' length scale and is the distance at which positional correlation begins to decay.[18] On length scales shorter than ξ_D, the topologically ordered lattice forms a quasi-Bragg glass (qBG). Such a qBG shows an exponentially sharp crossover to the high-temperature VL phase,[19] reminiscent of the ''melting'' transition of the pure system. A similar exponential crossover was proposed between the qBG and the VG phase as a function of B, or pinning strength.

The real-space structure of the vortex system has been studied using neutron diffraction[20–22] and Bitter decoration of vortices.[23–26] The latter technique allows direct visualization of the large-scale structure of the configuration and hence enables one to analyze the role of topological defects on the decay of translational order. Recent decoration experiments[25,26] of $NbSe_2$ have raised some important issues concerning the nature of the disordered phase. Previous transport measurements[27] on the same samples of $NbSe_2$ suggested an order-disorder transition on increasing B (or T). Fasano *et al.* showed that the spatial configuration of vortices does not show any significant difference between the ordered and the disordered vortex phases identified in Ref. 27. More importantly, both phases were found to be polycrystalline with dislocations forming grain boundaries. Within each grain, the lattice shows significant bond orientational order. This is in contrast to the naive theoretical picture of the ordered phase which expects a dislocation-free configuration, and the disordered phase in which the distribution of the dislocations is expected to be homogeneous.

In this paper, we analyze in detail the real-space configuration of the disordered phase using numerical simulation of a 2D vortex system at $T=0$. The magnetic field B is varied

over a wide range for various values of the pinning strength Δ. The real-space configuration shows that for the intermediate field range, the system shows inhomogeneous disordering. The majority of the dislocations are confined to the grain boundaries which forms the domain wall between regions of ordered lattice. The domain size and its distribution is dependent on B and Δ. We refer the intermediate fields in which the vortex state is quasiordered as the domain regime (DR). The DR is distinct from the amorphous regime at low fields and high fields, where the defects appear at a length scale $\sim a_0$ (lattice constant) and its distribution is homogeneous over the entire system. Analysis of the real-space images suggests domain wall roughening as a possible mechanism for the crossover between the DR and the high-fields amorphous regime. We also obtained the roughening exponent ζ of the vortex lattice in the domain regime. Finite-temperature simulation shows that the domain regime undergoes a sharp crossover to the high-T liquid phase, which is reminiscent of the thermal melting in the pure vortex system.

The paper is organized as follows. In Sec. II, we discuss the simulation approach in detail. The results and the analysis of the real-space configuration are presented in Sec. III, followed by conclusions in Sec. IV.

II. SIMULATION METHOD

We consider a 2D cross section perpendicular to the magnetic field $\mathbf{B}=B\hat{\mathbf{z}}$ of a bulk type-II superconductor in the mixed state. Within London's approximation, the vortex can be considered as a point particle with the dynamics governed by an overdamped equation of motion

$$\eta\frac{d\mathbf{r}_i}{dt}=-\sum_{j\neq i}\nabla U^v(\mathbf{r}_i-\mathbf{r}_j)-\sum_k\nabla U^p(\mathbf{r}_i-\mathbf{R}_k)+\mathbf{F}_{ext}+\boldsymbol{\zeta}_i(t). \tag{1}$$

Here, η is the flux-flow viscosity. On the left-hand side, the first term represents the intervortex interaction $U^v(r)=(\phi_0^2/8\pi^2\lambda^2)K_0(\tilde{r}/\lambda)$, where K_0 is the zeroth-order Bessel function, and $\tilde{r}=(r^2+2\xi^2)^{1/2}$. ϕ_0 is the flux quantum, and the λ and ξ are the penetration depth and the coherence length of the superconductor, respectively. This form of the intervortex interaction includes the finite core size of the vortex.[28] The second term represents vortex pinning by parabolic potential wells, where $U^p(r)=U_0(r^2/r_p^2-1)$ for $r<r_p$, and 0 otherwise. The pinning centers are randomly located at positions $\mathbf{R}_k$ in the simulation box. The third term $\mathbf{F}_{ext}=(1/c)\mathbf{J}\times\phi_0\hat{\mathbf{z}}$ is the Lorentz force experienced by the vortex due to the transport current density $\mathbf{J}$. The thermal noise is represented by $\boldsymbol{\zeta}$ with $\langle\zeta_{i,p}(t)\rangle=0$, and $\langle\zeta_{i,p}(t)\zeta_{j,p'}(t')\rangle=2k_BT\eta\delta_{ij}\delta_{pp'}\delta(t-t')$, where T is the temperature, k_B is the Boltzmann constant, and $p,p'=x,y$. The length is in units of $\lambda(B=0,T=0)=\lambda_0$, and the temperature T is in units of $\lambda_0 f_0/k_B$, where $f_0=\phi_0^2/8\pi^2\lambda_0^3$. The current density J and the velocity v of the vortices are in units of cf_0/ϕ_0 and f_0/η, respectively. Also, the prefactor for the pinning potential U_0 is scaled by f_0/λ_0.

We use the reduced magnetic field $b=B/B_{c2}$, where the upper critical field $B_{c2}=\phi_0/2\pi\xi_0^2$ and $\xi_0=\xi(B=0,T=0)$. b is calculated from the lattice constant $a_0/\lambda_0=(4\pi/\sqrt{3})^{1/2}(1/\kappa^2 b)^{1/2}$. The Ginzburg-Landau parameter $\kappa=\lambda/\xi$ is an input to the simulation. The magnetic-field dependence of the length scales λ and ξ follows the relation $\lambda(b)=f(b)\lambda_0$ and $\xi(b)=f(b)\xi_0$, respectively. The renormalization factor $f(b)=(1-b^2)^{-1/2}$. This form of the renormalization factor is similar to the temperature dependence of ξ and λ in the Ginzburg-Landau theory[29] with T/T_c replaced by $(B/B_{c2})^2$. Similar form of the renormalization factor for λ have been used in Ref. 30. The parameters used in the simulation are $\kappa=10$ and $\lambda_0=1000$ Å, which are close to the values for the low-T_c superconductors, particularly $NbSe_2$. Periodic boundary conditions are imposed in both directions, and the minimum image convention is followed. The magnetic field b is varied by changing the size of the simulation box, keeping the number of vortices $N_v=4096$ fixed. Simulations were also performed using N_v between 800 and 1200, and for some parameters $N_v=6400$ was used to check for the finite-size effects. The U_0 is distributed randomly between $\Delta\pm0.01$, where $\Delta=\langle U_0\rangle$. The range of the pinning potential $r_p=\xi_0$. In this paper, we present results for pin density $n_p=2.315/\lambda_0^2$. For $T=0$, Eq. (1) is time integrated by the predictor-corrector scheme, and the finite-temperature simulation is performed using Heun's method.[31] The simulation at high vortex densities requires long computational time and parallel algorithms were employed to reduce the run time. Details of the implementation of the parallel algorithms can be found in Ref. 32.

The real-space configuration is characterized by the topological defect density n_d/λ_0^2 (number of defects per unit area of the simulation box). Below, we also use the defect fraction f_d, which is defined as the number of defects per vortex. The defects are defined as vortices with coordination number other than 6 and are identified by Delaunay triangulation of the real-space position of the vortices. In 2D systems, the vortices with coordination number 5 and 7 are disclinations. A 5-disclination and a 7-disclination separated by a distance a_0 forms a bound pair which is an edge dislocation. Over most of the field range, the fraction of free disclinations is negligibly small and the majority of the defects are edge dislocations. Hence, the defect density n_d is approximately twice the dislocation density in the system. The hexatic order in the system is quantified by the sixfold orientational order parameter $\Psi_6=|\Sigma_{\langle ij\rangle}e^{6\theta_{ij}}|$, where θ_{ij} is the angle between the nearest-neighbor vortices relative to a reference axis.

The simulation is performed by two different methods. In the first method, we start with a perfect vortex lattice and the driving current $I(\propto J)$ is reduced to 0 from a value much greater than the depinning current I_c. This is referred as the current annealing (CA) method. In the second method, the conventional thermal annealing (TA) is applied wherein the temperature T is reduced to 0 in small steps from the high-temperature liquid phase (also known as simulated annealing). Experimentally, the TA is equivalent to the field cooling procedure. We have shown previously[33] that the configuration obtained by CA is stable to small perturbations com-

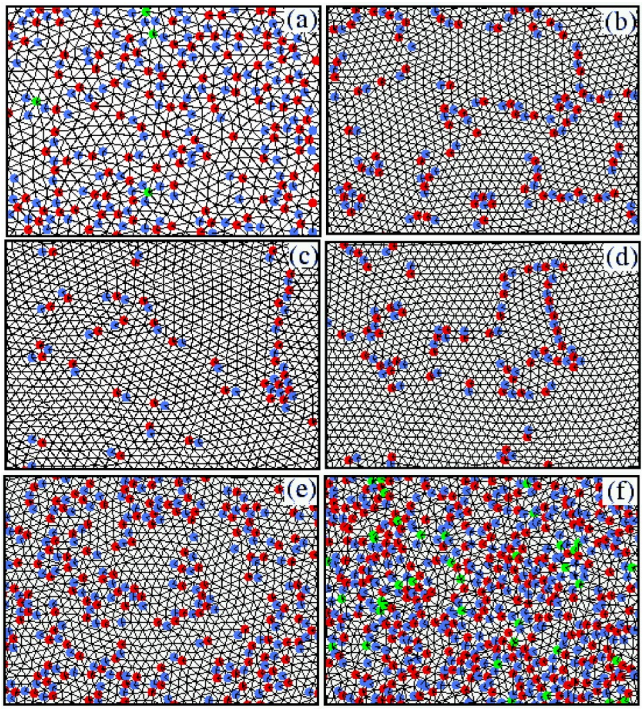

FIG. 1. (Color online) The real-space configuration of vortices in a region of the simulation box. The values of b are (a) 0.1, (b) 0.4, (c) 0.5, (d) 0.6, (e) 0.8, and (f) 0.9. The black (red) and gray (blue) dots denote vortices with seven and five neighbors, respectively (Ref. 35). For $b=0.1$, $N_v=900$, and for the rest of the images $N_v=4096$. The pinning strength $\Delta=0.02$.

pared to the configuration obtained by TA. This is also supported by experiments,[34] which show that the field cooled state is unstable to small driving force $I \ll I_c$ and a stable configuration is obtained when the system is brought to rest after driven with $I \gg I_c$. The two methods, CA and TA, are compared in Sec. III B.

III. RESULTS AND DISCUSSIONS

A. Zero-temperature simulation

In this section, we analyze the zero-temperature configurations obtained by the current annealing method. The system is slowly brought to rest across the depinning current for each value of the magnetic field b. In the absence of thermal fluctuations, the vortex configuration is determined by the balance between the long-range elastic force and the pinning force. We first show the real-space images of the configuration as the magnetic field b is increased.

1. Real-space configuration

Figure 1 shows the Delaunay triangulation in a region of the simulation box for various values of the magnetic field. The pinning strength $\Delta=0.02$, and $N_v=4096$, except for $b=0.1$ for which $N_v=900$. At small fields $b \lesssim 0.1$, the defect distribution is homogeneous over the entire system and the configuration is amorphous. The defect fraction (number of defects per vortex) $f_d > 0.35$ at these low fields.

With increasing b, small regions of ordered lattice start appearing. This can be seen for $b=0.1$ in which ordered lattice is formed in regions less than $3-4a_0$ wide. For $b \gtrsim 0.2$, the defect distribution becomes inhomogeneous. The dislocations come closer to form a network of grain boundaries across the system. For $b=0.4$ and $b=0.5$, we find that $\approx 90\%$ of the dislocations in the system are confined to the grain boundaries whereas $\approx 10\%$ of the dislocations are free within the domains. We also find that $\approx 5\%$ of the dislocations *within* the grain boundaries unbind into disclinations, which occurs generally at the intersection of the grain boundaries. Though the free disclinations are absent in the system, it does not lead to a long-range hexatic order in the system. For $b=0.6$, we find $\Psi_6 \approx 0.14$, and for other values of the field $\Psi_6 < 0.05$ (for a perfect vortex lattice, $\Psi_6=1$). The small value of Ψ_6 is caused by the random orientation of the domains which destroys the long-range orientational order.

We call the intermediate field range in which the system breaks into regions of ordered lattice the DR. The DR is configurationally distinct from the conventional picture of a disordered state for which the distribution of topological defects is homogeneous. In the DR, the system is quasiordered on the length scale of the domain size R_d. The vortex lattice shows translational and orientational order *within* the domains, even though the long-range order is absent in the system. Figures 1(b)–1(d) shows real-space configurations in the DR as b is increased.

For $b > 0.6$, the defect density increases rapidly with the concomitant decrease in the domain size. Small domains of ordered lattice of width $3-4a_0$ can be seen until $b \approx 0.8$, as evident from Fig. 1(e). Increasing $b \gtrsim 0.8$, the system becomes amorphous with an average distance $\sim a_0$ between the defects. The defect distribution is homogeneous throughout the system, and the configuration is similar to a frozen liquid. A typical real-space configuration is shown in Fig. 1(f). The fraction of free disclinations is significantly higher than that observed in the DR but it is difficult to isolate them from the dense network of defects. The vortices with coordination number 4 and 8 accounts for $\approx 6-8\ \%$ of the total defects. Overall, the real-space images in Fig. 1 suggests a reentrant change in the configuration, from a low-field amorphous to an intermediate field quasiordered state, which finally crosses over to a high-field amorphous state.

In the DR, the average domain size R_d is dependent on b and Δ. $R_d \approx 5-7a_0$ for low fields and increases in the intermediate field range. For $b=0.6$ and $\Delta=0.02$, the size of some domains exceeds $20a_0$. By decreasing the pinning strength Δ to 0.01, we find a remarkably well-ordered lattice with no topological defects for the system size $N_v=6400$, as shown in Fig. 2(a). This suggests that for sufficiently weak pinning strength, large domains of ordered lattice, comparable to sample size in typical experiments, can exist in 2D. Figure 2(a) should be compared with Fig. 2(b) which shows the meandering grain boundaries formed by the defects for $\Delta=0.02$. With increasing Δ, R_d decreases from $\approx 20a_0$ for $\Delta=0.02$ to $\approx 3-5a_0$ for $\Delta=0.075$. This is shown in Fig. 3. For strong pinning, the dislocations tend to cluster in some regions implying that individual pinning centers locally tear the vortex lattice. With increasing Δ, the field range over

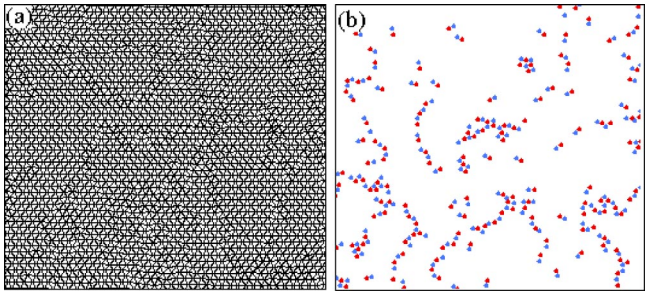

FIG. 2. (Color online) The real-space configuration of vortices in a region of the simulation box for $\Delta = 0.01$ (a), and 0.02 (b). The $N_v = 6400$. In (b), only the defects are shown.

which the DR exists is reduced and in the strong pinning limit, the system is amorphous for all values of b.

In recent experiments, the changes in the real-space configuration of vortices were studied in weak pinning $NbSe_2$ samples across the order-disorder transition by the Bitter decoration technique.[25,26] The order-disorder transition was previously identified in transport measurements and have been speculated to underly the peak effect in the critical current density.[27] The decoration images show that the vortices form large ordered domains. The domains are separated by domain walls, which are defined by chains of dislocations. This domain formation is present throughout the B-T plane (below the melting line), hence the authors summarized their findings as the ''absence of amorphous vortex matter.'' Fasano *et al.* found that ≈ 85–$90\,\%$ of the defects are in the grain boundaries, whereas the remaining defects are isolated dislocations. All of these findings are consistent with our numerical findings and estimates in the intermediate field range for $\Delta = 0.02$.

2. Domain size distribution

A useful quantity to characterize the DR is the distribution of the domain size $N(s_d)$, where the area of the domain s_d is in units of a_0^2. Unlike in lattice models, extracting $N(s_d)$ in models with continuous symmetry is not straightforward. The lattice vectors can change continuously from domain to neighboring domain *without* nucleating defects, which makes it difficult to define the domain wall. In many cases, the domain walls, which are formed by the grain boundaries are not closed. Analysis of the real-space configuration suggests that the domain walls are generally composed of two types of grain boundaries, depending on the misorientation angle θ_d between the neighboring domains. For the small-angle grain boundaries, $\theta_d \sim 10°$–$16°$, and the dislocations are separated by 3–$5a_0$. In large-angle grain boundaries, the dislocations form closely packed stringlike structures, and $\theta_d > 20°$. Typical domains and domain walls formed by the grain boundaries are shown in Fig. 4.

To extract $N(s_d)$, we used the following procedure to define domain walls in regions where the dislocations are apart. The misorientation angle θ_d is obtained between successive vortices along one of the lattice vectors connecting neighboring domains. If θ_d is between 12° and 18°, then the vortex is considered as part of the domain wall. With this

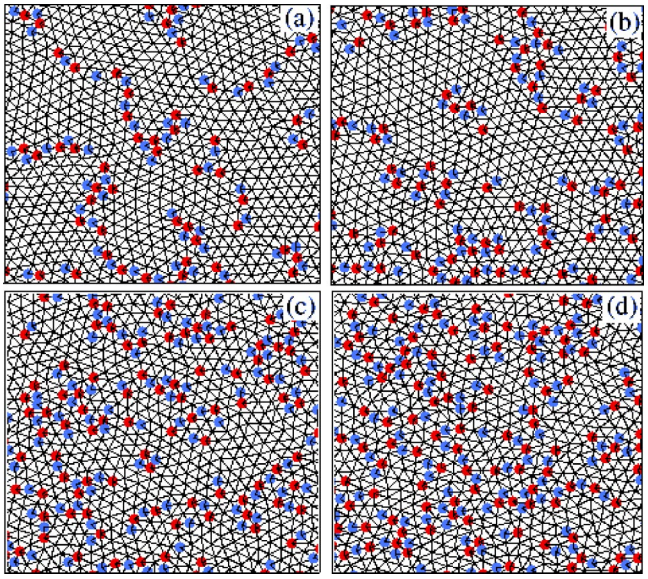

FIG. 3. (Color online) The vortex configuration in a region of the simulation box for $b = 0.6$ and for $\Delta = 0.03$ (a), 0.04 (b), 0.05 (c), and 0.075 (d). The number of vortices $N_v = 4096$.

method, the domain boundary in many cases could be determined with reasonable accuracy. This procedure is intended to be instructive rather than decisive, as it contains some arbitrariness. For example, in some regions the domain walls are wider than a_0 and then the misorientation angle is split across the domain wall. Also, this method does not count the really small-angle domain walls, those with $\theta < 12°$.

The area of the enclosed domains is used in creating the $N(s_d)$ histogram. Figure 5 shows the histogram plot of $N(s_d)$ for various values of the magnetic field b. The total number of vortices $N_v = 4096$ and $\Delta = 0.02$. At small and large fields, the histogram can be adequately characterized by a single parameter, e.g., its half width. The distribution is relatively narrow with few large domains. For the intermediate fields, the $N(s_d)$ exhibits a broad distribution with substantial weight toward the tail region. This suggests that

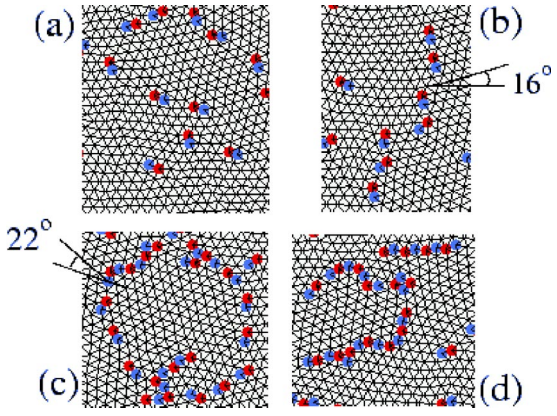

FIG. 4. (Color online) The domain walls in the real-space configuration. (a) and (b) shows small angle grain boundaries, whereas large angle grain boundaries can be seen in (c) and (d). The magnetic field $b = 0.50$ for (a) and (d), and 0.65 for (b) and (c).

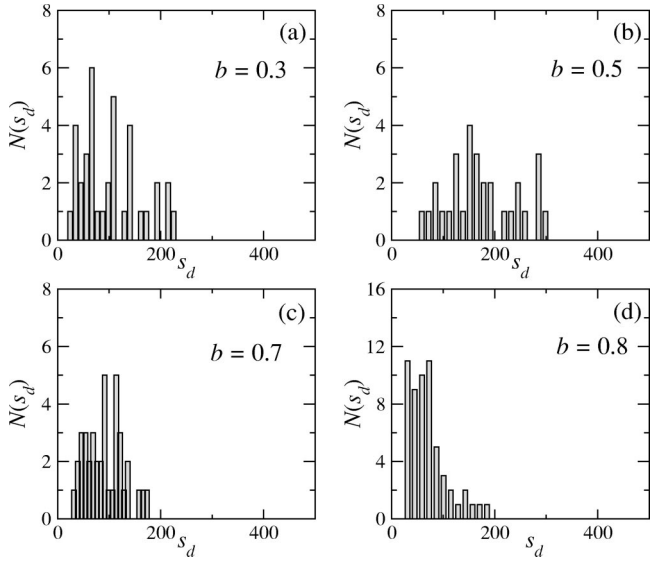

FIG. 5. The histogram plot of the domain size distribution $N(s_d)$, where s_d is in the units of a_0^2. The values of b are (a) 0.3, (b) 0.5, (c) 0.7, and (d) 0.8. The $N_v=4096$ and $\Delta=0.02$.

more than one parameter is required to characterize these distributions, especially the excess weight in the tail region.

3. Roughness exponent

The interaction of the vortex lattice with the quenched impurities leads to displacement of the vortices from their perfect lattice position. An important quantity which characterize the change in the position of the vortices is the relative displacement correlation, defined as

$$W(\mathbf{r})=\overline{[\mathbf{u}(\mathbf{r})-\mathbf{u}(0)]^2}, \tag{2}$$

where the overbar represents the average over quenched impurities. The $\mathbf{u}(\mathbf{r})$ is the displacement of the vortex relative to its position in the perfect lattice. The positional order-parameter correlations $C_{\mathbf{G}}(r)$ can be expressed in terms of $W(r)$ as $C_{\mathbf{G}}(r)\sim e^{-G^2W(r)/2}$, where $\mathbf{G}$ is one of the reciprocal lattice vectors.[3] For the crystalline state, $W(r)=0$ and $C_{\mathbf{G}}(r)=1$. The effect of the quenched impurities is to increase $W(r)$ and hence reduce the positional order-parameter correlations of the lattice. The structure factor at $\mathbf{G}$, measured in the neutron-scattering experiments, is related to the Fourier transform of $C_{\mathbf{G}}(r)$.

The roughness of an elastic medium is parametrized by the exponent ζ, which is defined as $W(r)\sim r^{2\zeta}$. In the flat phase of the medium $\zeta<0$, and in the rough phase $\zeta>0$ [the $\zeta=0$ gives logarithmic roughening with $W(r)\sim\ln r$]. For a 2D vortex system, there are three length scales which emerge in various theories depending upon the displacement $u(r)$.

(1) $r<R_c$: In the collective pinning theory[6] R_c represents the size of the region in which the vortex lattice is coherently pinned by the impurities. More precisely, R_c is the length scale at which the displacement $u(r=R_c)\sim\xi$. R_c is obtained by minimizing the total energy (elastic energy + pinning energy) and is given by

$$R_c\approx\frac{C_{66}\xi}{fn_p^{1/2}}. \tag{3}$$

The C_{66} is the shear modulus of the vortex lattice and the average pinning force $f\sim\Delta/r_p$, where r_p is the range of the pinning potential as defined in Sec. II. For the $K_0(r/\lambda)$ potential, the field dependence of the shear modulus have been derived[36] and is given as $C_{66}\approx\phi_0B/(4\pi\lambda)^2(1-b)^2$. In dimensionless units, the R_c becomes

$$\frac{R_c}{a_0}\approx\frac{1}{(2\pi)^{3/2}}\frac{\kappa^2}{fn_p^{1/2}}b^{3/2}(1-b)^2. \tag{4}$$

The R_c increases with b and attains a maximum before decreasing as $b\to1$.

The $r<R_c$ regime is often referred as the random force (RF) regime. The roughness exponent in this regime is given by $\zeta=4-D/2$ for a D-dimensional system. Thus, $\zeta_{RF}^{2D}=1$ and $\zeta_{RF}^{3D}=0.5$ for $2D$ and $3D$ systems, respectively.

(2) $R_c<r<R_a$: Beyond R_c, the displacement $u(r)$ continues to grow but with smaller exponent. R_a defines the length scale at which the positional correlation begins to decay, i.e., the displacement $u(r=R_a)\sim a_0$. Between R_c and R_a, the system is in the random manifold (RM) regime. In this regime, the roughness exponent have been obtained using a Flory type argument[37,38] which gives $\zeta_{RM}^{2D}=\frac{1}{3}$. A more refined scaling argument[39] gives $\zeta_{RM}^{2D}=0.4$. For weak pinning, the length scales R_a and R_c are related by $R_a\sim R_c(a_0/\xi)^{1/\zeta_{RM}}$.

(3) $R_a<r<\xi_D$: Beyond R_a, $W(r)$ grows as[3,4] $W(r)\sim\ln^2(r)$ as derived through a variational approach and confirmed by replica symmetric RG (Ref. 41), assuming the lack of dislocations at these scales.[40] This growth form holds up to the length scale ξ_D, at which unbound dislocations appear. For weak pinning, $\xi_D\gg R_a$,[18]

$$\xi_D\sim R_a\exp\left[c\sqrt{\left(\frac{1}{8}-\sigma_0\right)\ln\left(\frac{R_a}{a_0}\right)}\right], \tag{5}$$

where c is a temperature-dependent numerical constant and σ_0 is the impurity strength. For $R_a\gg a_0$ and low temperatures, ξ_D can become exceedingly large and the system appears similar to the BG phase in 3D.

(4) $\xi_D<r$: Beyond ξ_D, unbound dislocations lead to exponential decay of the positional correlation and the system is disordered.

We have obtained the length scale and the roughness exponent of the vortex lattice in the DR. The relative displacement correlation $W(r)$ was calculated using the following procedure. First, a crystalline state with the lattice constant corresponding to the value of b is constructed using one of the vortex coordinates $\mathbf{r}_0$ in the real lattice as the origin. The mean-square displacement between the perfect lattice and the underlying real lattice is then minimized by varying the orientation of the perfect lattice relative to the real lattice. The $u(r)$ is then computed for each of the vortices. This procedure is repeated for different $\mathbf{r}_0$'s, and the $W(r)$ is computed by averaging over all $\mathbf{r}_0$'s.

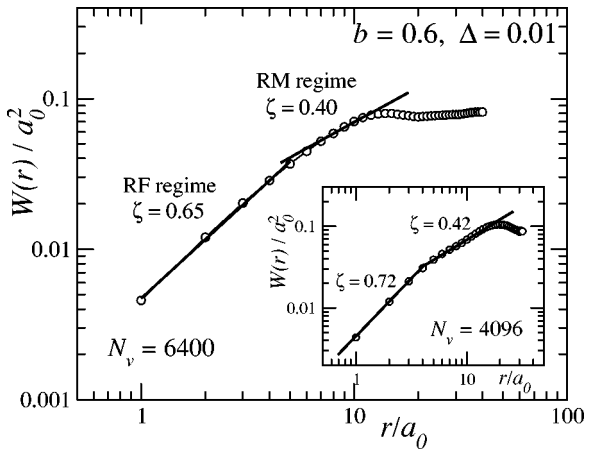

FIG. 6. The $W(r)/a_0^2$ as a function of r/a_0 for $\Delta=0.01$ for $N_v=6400$. The inset shows the same for $N_v=4096$. The $W(r)\sim r^{2\zeta}$ where the exponent ζ is shown for the RF regime and the RM regime.

Figure 6 shows the plot of $W(r)/a_0^2$ for $b=0.6$ and $\Delta=0.01$ for $N_v=6400$. $W(r)$ for $N_v=4096$ is shown in the inset. For these parameters, even the largest $N_v=6400$ system is free of dislocations [see Fig. 2(a)]. Due to periodic boundary condition, the length scale probed in the simulation is half the system size, which for $N_v=6400$ and 4096 are $40a_0$ and $32a_0$, respectively. $W(r)$ shows an initial power-law increase with an exponent $\zeta\approx 0.65$–0.72. The system exhibits a crossover around $r^*\approx 4$–$5a_0$ into a regime where the increase of $W(r)$ is slower. Between $5a_0\lesssim r\lesssim 15a_0$ the exponent is $\zeta\approx 0.40$–0.42. For $r\gtrsim 16a_0$, the growth of $W(r)$ slows down considerably.

It is plausible that $r^*=R_c$, where the system crosses over from the RF regime to the RM regime. This can be verified by calculating R_c using Eq. (4), which gives a value $\approx 4a_0$ for $b=0.6$, in reasonable agreement with the value of r^*. In our system $\xi=0.1\lambda_0$, and at $b=0.6$ the lattice constant $a_0=0.347\lambda_0$. From Fig. 6, $u(R_c)\approx 0.2a_0\approx 0.07\lambda_0$, thus confirming that $u(r=R_c)\approx\xi$.

Beyond R_c, the length scale R_a of the RM regime is defined as $u(r=R_a)\sim a_0$. This translates to $W(r)\approx 0.12a_0^2$ for $b=0.6$. From Fig. 6, we find that $W(r)$ flattens at ≈ 0.1 at $r\sim 13a_0$ for $N_v=6400$, which suggests that $R_a\approx 13a_0$ (for $N_v=4096$, $R_a\approx 18a_0$). Beyond R_a, the slow growth of $W(r)$ indicates the appearance of the asymptotic regime. Within the qBG theory,[3] $W(r)$ is expected to grow as $\ln^2(r)$ in the asymptotic regime. This behavior unfortunately could not be verified due to insufficient range of data points. In sum, we identify the $r\sim 1a_0$–$5a_0$ as the RF regime, the $r\sim 5a_0$–$15a_0$ as the RM regime, and $r>15a_0$ as the asymptotic regime.

The value of $\zeta\approx 0.65$–0.72 obtained from the simulation in the RF regime is smaller than the theoretical prediction for $\zeta_{RF}^{2D}=1$. We speculate that the interaction $K_0(r/\lambda)$ between the vortices in 2D increases the stiffening of the vortex lattice at short distances which leads to weaker roughening. In the RM regime, the exponent $\zeta\approx 0.40$–0.42 is in good agreement with the value of 0.4 expected from the scaling argument.[39] Using $\zeta_{RM}^{2D}=0.4$, the value of $R_a\approx 15a_0$ is much smaller than the value $R_a\sim R_c(a_0/\xi)^{1/\zeta_{RM}^{2D}}$. The small size of the RM regime is possibly related to the large magnetic field $b=0.6$ used in obtaining $W(r)$. For this field, a_0 is comparable to ξ, and R_c is large compared to smaller magnetic fields. The RM regime is expected to disappear for $a_0=\xi$, and have been shown in the case of 3D system.[42]

An interesting outcome of the above analysis of $W(r)$ is that the average domain size $R_d\gg R_c$, and hence, the collective pinning theory cannot account for the appearance of domains in the intermediate fields. The asymptotic regime in $W(r)$ suggests that the qBG theory is qualitatively correct. Within the qBG theory, the distribution of dislocations beyond the length scale ξ_D is expected to be homogeneous, unlike the grain-boundary formation observed in our simulation. One possible way to account for the grain-boundary formation is to consider the long-range interaction between the dislocations. Since the interaction between the dislocations is anisotropic, for some values of dislocation density, the grain boundaries may lead to a lower-energy state. This is also supported from a recent work on dipole systems.[43] At low densities, the dipoles exhibit a gaseous phase, and their distribution is roughly homogeneous. At higher densities the phase is characterized by dipoles forming chains or strings. Since the dislocations of the vortex lattice are in fact dipoles of disclinations, these results are quite analogous to our identification of a domain regime in the vortex matter.

4. Defect density

The three field regimes discussed in the context of the real-space configuration can also be inferred from the behavior of the defect density $n_d(b)$. Figure 7(a) shows $n_d(b)$ for $\Delta=0.02$ and $N_v=4096$. The behavior for smaller system

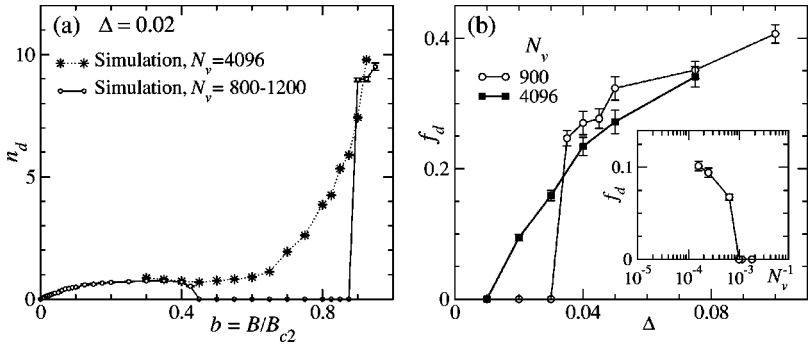

FIG. 7. (a) The topological defect density $n_d(b)$ for $\Delta=0.02$ and $N_v=4096$. Also shown is the $n_d(b)$ for the smaller system size. (b) The $f_d(\Delta)$ for $b=0.6$. Inset: The plot of f_d as a function of N_v^{-1} for $\Delta=0.02$ and $b=0.6$. There is a critical system size below which dislocations are not present in the system.

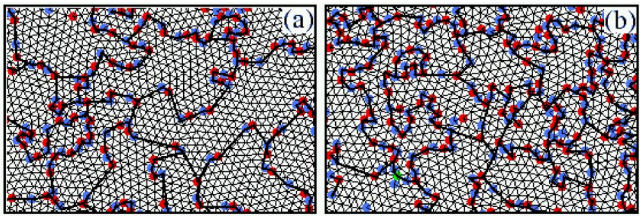

FIG. 8. (Color online) The domains in a region of the simulation box for (a) $b=0.7$ and (b) 0.8. The $N_v=4096$ and $\Delta=0.02$.

sizes ($N_v=800-1200$) is also shown on the same plot. The $n_d(b)$ increases linearly in the low-field amorphous regime. Above a crossover field $b_l \approx 0.1$, $n_d(b)$ flattens and becomes weakly field dependent in the DR. For $b \gtrsim 0.6$, $n_d(b)$ increases rapidly, and above $b_h \approx 0.8$ the system crosses over to the high-field amorphous regime. It is possible to define a length scale $L_d \sim n_d^{-1/2}$, as the nominal average defect separation. For $b=0.6$ (domain regime) $L_d \approx 3a_0$, which is much smaller than even R_c and does not correspond to any feature in the real-space configuration, and reflects the highly inhomogeneous nature of the defect distribution in the domain regime. On the other hand, in the high-field amorphous regime $L_d \sim a_0$, which is also the distance between the defects, thus reflecting homogeneity of the distribution of defects.

The $n_d(b)$ in Fig. 7(a) shows strong similarity with the experimental observation in 2D system of magnetic bubbles.[44] In Ref. 44, the intermediate regime was interpreted as the hexatic phase and the high-field amorphous regime as the isotropic liquid phase.[45] Later simulation[46] also suggested a $T=0$ dislocation unbinding transition driven by disorder. As discussed above, the presence of domain walls (grain boundaries) in our system suppresses the long-range orientational order. This rules out the possibility of a transition between the hexatic phase and the isotropic liquid phase as the underlying reason for the rapid increase in $n_d(b)$. However, a rapid crossover, similar to that predicted between the qBG at low temperatures and vortex liquid at high temperatures,[19] is still possible between the DR and the high-field amorphous regime, especially at weaker pinning where the domain size R_d is large.[47]

For smaller system size ($N_v=800-1200$), a topologically ordered phase appears in the intermediate field range in which $n_d=0$ [see Fig. 7(a)]. This is a finite-size effect, which reflects the sensitivity of the DR to the system size L. For $L<\xi_D$, the DR can appear as a topologically ordered state free of dislocations. This implies that for a given system size, there exists a critical Δ_c below which dislocations are not favored. This is observed in the simulation, as shown in Fig. 7(b) where the defect fraction $f_d(\Delta)$ (number of defects per vortex) is plotted for $b=0.6$. For the smaller system $N_v=900$, f_d goes to zero at $\Delta_c=0.03$, and the system exhibits an ordered phase for $\Delta<\Delta_c$. Increasing N_v to 4096 reduces Δ_c to 0.01, and in the asymptotic limit $N_v \to \infty$ (hence, $L \to \infty$), we expect $\Delta_c \to 0$. In the DR, f_d does not increase continuously with increasing $L(\propto N_v^{1/2})$ but shows a sharp jump from the dislocation-free state to the domain state at a characteristic system size as shown in the inset of Fig. 7(b).

5. Crossover from DR to high-field amorphous regime

As discussed above, the $n_d(b)$ shows a rapid crossover from the DR to the high-field amorphous regime. To understand the mechanism for this sharp crossover, we identified the domains and the domain walls between $b=0.5$ and $b=0.8$ for $\Delta=0.02$. For the intermediate fields $b \approx 0.5-0.6$, the grain boundaries are generally smooth and $n_d(b)$ is weakly field dependent. For $b \gtrsim 0.6$, the rapid increase in $n_d(b)$ occurs *within* the domain walls. Consequently, the domain wall length increases, which is accommodated through enhanced roughening of the domain walls. This is evident from Fig. 8(b). The increase in the roughening also facilitates the unbinding of the dislocations into free disclinations and subsequently drives the crossover into the VG state. In such a scenario, we conjecture that domain walls undergo disorder driven roughening transition at the crossover between the DR and the high-field VG. It would be of interest to obtain the domain-wall roughening exponent across the crossover regime.

B. Finite-temperature simulation

In this section, we compare the current annealing method with the conventional simulated annealing method, as it is well known that different sample preparation techniques can result in the vortex system not reaching its equilibrium configuration.[33,48] In the latter method, the temperature T is reduced from the high-temperature liquid phase slowly so as to reach thermal equilibrium at each value of T. This method is commonly used to search for the ground state of disordered systems.

For the thermal annealing, the system was equilibrated for $5\times10^4-1\times10^5$ time steps before averaging over a similar time scale to calculate the defect fraction $f_d(T)$. The number of vortices $N_v=900$ and $\Delta=0.03$. For this system size, the

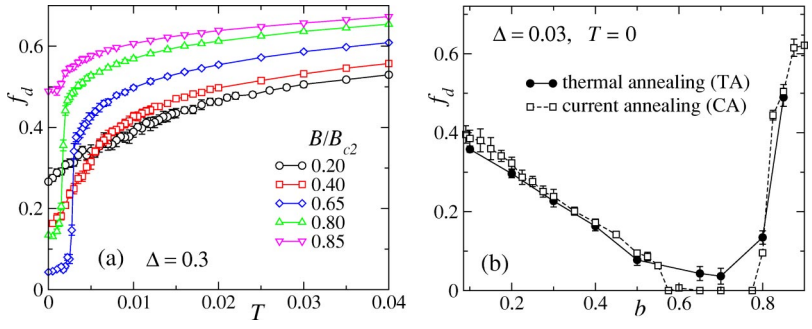

FIG. 9. (Color online) (a) The defect fraction $f_d(T)$ for various magnetic fields b with $\Delta=0.03$. The temperature T is decreased slowly from the high-T liquid phase. (b) The $f_d(b)$ at $T=0$ obtained from thermal annealing and current annealing.

CA method gives a topologically ordered phase for b between 0.6 and 0.75. Figure 9(a) shows $f_d(T)$ for various values of the magnetic field. As the temperature is lowered, for $b=0.2$ $f_d(T)$ decreases monotonically to a finite value with df_d/dT slowly varying. There is no evidence of a transition as a function of the temperature. With increasing b, the slow freezing is replaced by a sharp decrease in $f_d(T)$ at a particular temperature T_m, similar to the equilibrium melting transition. For $b=0.65$, $f_d(T)$ at T_m decreases by $\approx 76\%$ of the value above T_m. For $b>0.8$, the meltinglike transition is again replaced by slow freezing of the high-temperature liquid phase.

In Fig. 9(b), $f_d(b)$ at $T=0$ obtained by TA is compared with that obtained by CA. At intermediate fields, the thermally annealed samples exhibit the presence of dislocations already at these smaller system sizes. As described above, the current annealing method requires larger system sizes to correctly display this same phenomenon. Otherwise, the two curves track each other very closely over most of the field range, including the low-field slow decay of $f_d(b)$ and the rapid rise at high fields. For the intermediate fields, the $T=0$ configuration obtained from TA also shows grain-boundary formation, similar to that observed from the CA method.

IV. CONCLUSION

We have presented a detailed numerical analysis of the real-space configuration of 2D vortex system in the presence of quenched impurities. For weak pinning, the disordered state in the intermediate field range is inhomogeneous. The majority of the dislocations in this state are confined to grain boundaries, which form domain walls between regions of topologically ordered vortex lattice. There are no free disclinations in the system. This state is referred as the domain state and the intermediate field range as the domain regime.

The domain size distribution $N(s_d)$ was calculated in the domain regime. $N(s_d)$ shows a broad distribution with a large weight in the tail region at intermediate fields. Therefore, more than one length scale is required to properly characterize the domain size distribution in the domain regime. With increasing b, the distribution becomes narrow and the peak shifts toward the origin. For weak pinning, the size of the domains can become exceedingly large.

The domain regime is bounded by an amorphous regime at low fields and high fields. The defects in the amorphous regime are separated by the smallest length scale $\sim a_0$ and show homogeneous distribution unlike the grain-boundary formation in the domain regime. The domain regime shows rapid crossover into the high-field amorphous regime. From the changes in the configuration, we identified the roughening of the domain walls as the plausible mechanism driving the rapid crossover.

The relative displacement correlation $W(r)$ in the domain state was also calculated for weak pinning. Three distinct regimes were observed: a random force regime, a random manifold regime, and the asymptotic regime. Crossover from random force regime to the random manifold regime is found to occur at $R_c \sim 4-5a_0$. The value of R_c agrees with that obtained from the collective pinning theory. The roughness exponent ζ in the random manifold regime is found to ≈ 0.40, within the range of various theoretical predictions.

The observation of random manifold and asymptotic regimes *within* the domains for weak pinning suggests that the vortex lattice is correctly described by the qBG idea, though the exact form of the $W(r)$ could not be ascertained. At length scales greater than the domain size, the appearance of the domain wall formed by dislocations is not captured by the quasi-Bragg glass theory. Therefore, it remains to be seen whether besides the domain regime the 2D vortex matter supports a quasi-Bragg glass where the dislocations are homogeneously distributed.

ACKNOWLEDGMENTS

M.C. acknowledges useful discussions with E. Zeldov and A. K. Grover during the course of the work. G.T.Z. thanks Y. Fasano, T. Giamarchi, J. Kierfeld, P. Le Doussal, and T. Nattermann for insightful discussions. M.C. would also like to thank the University of New Mexico for access to their Albuquerque High Performance Computing Center. The simulation was performed on the UNM-Alliance Supercluster. This work was supported by NSF-DMR Grant No. 9985978.

*Corresponding author. Present address: Jawaharlal Nehru Centre for Advanced Scientific Research, Jakkur, Bangalore 560064, India. Electronic address: mchandran@physics.iisc.ernet.in

[1] An ensemble of vortex line is referred as the $3D$ vortex system, whereas the $2D$ vortex system refers to pancake vortices confined within a plane.

[2] G. Blatter, M.V. Feigel'man, V.B. Geshkenbein, A.I. Larkin, and V.M. Vinokur, Rev. Mod. Phys. **66**, 1125 (1994).

[3] T. Giamarchi and P. Le Doussal, Phys. Rev. Lett. **72**, 1530 (1994); Phys. Rev. B **52**, 1242 (1995).

[4] T. Nattermann and S. Scheidl, Adv. Phys. **49**, 607 (2000), and references therein.

[5] The term ''impurity'' is used for the quenched disorder, which provides the pinning potential for the vortices. The term ''disorder'' is used to identify the state of the vortex configuration in real space.

[6] A.I. Larkin, and Yu.N. Ovchinnikov, J. Low Temp. Phys. **34**, 409 (1979).

[7] D.S. Fisher, M.P.A. Fisher, and D.A. Huse, Phys. Rev. B **43**, 130 (1990).

[8] See also T. Nattermann, Phys. Rev. Lett. **64**, 2454 (1990); S.E. Korshunov, Phys. Rev. B **48**, 3969 (1993).

[9] T. Emig, S. Bogner, and T. Nattermann, Phys. Rev. Lett. **83**, 400 (1999).

[10] D.S. Fisher, Phys. Rev. Lett. **78**, 1964 (1997).

[11] The vortex glass phase proposed by Fisher *et al.* in Ref. 7 is expected to show long-range phase coherence. Here, we use the term VG for the generic phase where dislocations appear at the smallest length scale, i.e., $\xi_D \sim a_0$.

[12] T. Giamarchi and P. Le Doussal, Phys. Rev. B **55**, 6577 (1997).

[13] D. Ertaş and D. Nelson, Physica C **272**, 79 (1996).
[14] V. Vinokur, B. Khaykovich, E. Zeldov, M. Konczykowski, R.A. Doyle, and P.H. Kes, Physica C **295**, 209 (1998).
[15] A.E. Koshelev and V.M. Vinokur, Phys. Rev. B **57**, 8026 (1998).
[16] C. Zeng, P.L. Leath, and D.S. Fisher, Phys. Rev. Lett. **82**, 1935 (1999).
[17] M.J.P. Gingras, and D.A. Huse, Phys. Rev. B **53**, 15 193 (1996).
[18] P. Le Doussal and T. Giamarchi, Physica C **331**, 233 (2000).
[19] D. Carpentier and P. Le Doussal, Phys. Rev. Lett. **81**, 1881 (1998).
[20] I. Joumard, J. Marcus, T. Klein, and R. Cubitt, Phys. Rev. Lett. **82**, 4930 (1999).
[21] T. Klein, I. Joumard, S. Blanchard, J. Marcus, R. Cubitt, T. Giamarchi, and P. Le Doussal, Nature (London) **413**, 404 (2001).
[22] X.S. Ling, S.R. Park, B.A. McClain, S.M. Choi, D.C. Dender, and J.W. Lynn, Phys. Rev. Lett. **86**, 712 (2001).
[23] D.G. Grier, C.A. Murray, C.A. Bolle, P.L. Gammel, D.J. Bishop, D.B. Mitzi, and A. Kapitulnik, Phys. Rev. Lett. **66**, 2270 (1991).
[24] M. Marchevsky, A. Keurentjes, J. Aarts, and P.H. Kes, Phys. Rev. B **57**, 6061 (1998).
[25] M. Menghini, Y. Fasano, and F. de la Cruz, Phys. Rev. B **65**, 064510 (2002).
[26] Y. Fasano, M. Menghini, F. de la Cruz, Y. Paltiel, Y. Myasoedov, E. Zeldov, M.J. Higgins, and S. Bhattacharya, Phys. Rev. B **66**, 020512(R) (2002).
[27] Y. Paltiel, E. Zeldov, Y. Myasoedov, M.L. Rappaport, G. Jung, S. Bhattacharya, M.J. Higgins, Z.L. Xiao, E.Y. Andrei, P.L. Gammel, and D.J. Bishop, Phys. Rev. Lett. **85**, 3712 (2000).
[28] J.R. Clem, J. Low Temp. Phys. **18**, 427 (1975).
[29] M. Tinkham, *Introduction to Superconductivity* (McGraw-Hill, New York, 1975).
[30] S. Ryu and D. Stroud, Phys. Rev. B **54**, 1320 (1996).
[31] A. Greiner, W. Strittmatter, and J. Honerkamp, J. Stat. Phys. **51**, 95 (1988).
[32] Mahesh Chandran, cond-mat/0103263 (unpublished).
[33] Mahesh Chandran, R.T. Scalettar, and G.T. Zimányi, Phys. Rev. Lett. **89**, 187001 (2002).
[34] W. Henderson, E.Y. Andrei, M.J. Higgins, and S. Bhattacharya, Phys. Rev. Lett. **77**, 2077 (1996).
[35] Few vortices have 8 or 4 neighbors in (a) and (f) and is shown by green dots. We have not attempted to distinguish it in the gray scale for the sake of clarity.
[36] E.H. Brandt, Rep. Prog. Phys. **58**, 1465 (1995).
[37] M. Kardar, J. Appl. Phys. **61**, 3601 (1987).
[38] T. Nattermann, Europhys. Lett. **4**, 1241 (1987).
[39] M.V. Feigel'man, V.B. Geshkenbein, A.I. Larkin, and V.M. Vinokur, Phys. Rev. Lett. **63**, 2303 (1989).
[40] The dislocation-free behavior in 2D at long length scale have been studied previously in the context of roughening transition of the crystal surface. See J. Toner and D.P. DiVincenzo, Phys. Rev. B **41**, 632 (1990).
[41] D. Carpentier and P. Le Doussal, Phys. Rev. B **55**, 12 128 (1997).
[42] S. Bogner, T. Emig, and T. Nattermann, Phys. Rev. B **63**, 174501 (2001).
[43] T. Tlusty and S.A. Safran, Science **290**, 1328 (2000).
[44] R. Seshadri and R.M. Westervelt, Phys. Rev. B **46**, 5150 (1992).
[45] D.R. Nelson and B.I. Halperin, Phys. Rev. B **19**, 2457 (1979).
[46] Min-Chul Cha and H.A. Fertig, Phys. Rev. Lett. **73**, 870 (1994); see also **74**, 4867 (1995).
[47] Smaller system size ($N_v = 800-1200$), for which an ordered phase appears at intermediate fields for weak pinning, shows a sharp first-order like transition to the high-field amorphous phase.
[48] M. Nicodemi and H. Jensen, J. Phys. A **34**, 8425 (2001).